JOURNAL OF SPACECRAFT AND ROCKETS
Vol. 39, No. 1, January–February 2002

Flutter Analysis of a Wraparound Fin Projectile Considering Rolling Motion

Seung-Kil Paek,* Jae-Sung Bae,† and In Lee‡
Korea Advanced Institute of Science and Technology, Taejon 305-701, Republic of Korea

The aeroelastic stabilities of curved fins (or wraparound fins) in rolling motion are investigated in the supersonic flow region. Because of their inherent roll, wraparound fins are subjected to both aerodynamic and centrifugal forces. The aerodynamic force is computed by solving Euler equations in a body-fixed rotating coordinate frame. The normal mode analyses of the spinning structure are performed by using a multipurpose finite element code. For the consistent analysis a nondimensionalized aeroelastic equation considering the rolling motion is derived and aeroelastic parameters, such as velocity index and mass ratio, are devised. From the flutter analyses for wraparound fins, it is observed that the flutter characteristics with roll are very different from those without roll. It indicates that the consideration of the rolling motion must be made to predict the flutter stability accurately. Because of the geometric asymmetry of the wraparound fin, the flutter characteristics in each roll directions are different from each other. Flutter analyses indicate that there exists a more stable roll direction for flutter.

Nomenclature

A	=	area associated with ΔC_p
C_{ij}	=	aerodynamic influence coefficient
D	=	reference diameter
$\hat{E}, \hat{F}, \hat{G}$	=	contravariant flux vectors in generalized coordinates
e	=	total energy, nondimensionalized by U_∞^2
h	=	enthalpy, nondimensionalized by U_∞^2
J	=	Jacobian
K	=	stiffness matrix
$\bar{K}$	=	nondimensionalized stiffness matrix
M	=	mass matrix
$\bar{M}$	=	nondimensionalized mass matrix
M_0	=	reference mass
M_∞	=	freestream Mach number
P_a	=	aerodynamic force vector
p	=	pressure, nondimensionalized by $\rho_\infty U_\infty^2$
p_∞	=	freestream static pressure
$\hat{Q}$	=	conservative flow variable vector
$\hat{S}$	=	source vector due to rotating coordinate frame
U, V, W	=	contravariant velocities along the generalized coordinates
U_∞	=	freestream flow speed
u, v, w	=	Cartesian velocity components, nondimensionalized by U_∞
u_s	=	structural displacement, deflection
V_I	=	velocity index, defined as $U_\infty/\omega_0 D\sqrt{\mu}$
V_{ID}	=	divergence velocity index
V_{If}	=	flutter velocity index
x, y, z	=	Cartesian coordinates, nondimensionalized by D
ΔC_p	=	pressure coefficient difference
μ	=	mass ratio, defined as $2M_0/\rho_\infty D^3$
ξ, η, ζ	=	generalized coordinates
ρ	=	density, nondimensionalized by ρ_∞
ρ_∞	=	freestream density
$[\Psi]$	=	modal matrix
$\{\psi\}_i$	=	modal vector in ith column of $[\Psi]$
$\bar{\Omega}$	=	roll rate
$\bar{\Omega}$	=	roll rate, nondimensionalized by ω_0
Ω^*	=	roll rate, nondimensionalized by U_∞/D
$\bar{\omega}_f$	=	flutter frequency
ω_0	=	reference frequency

Received 23 January 2001; revision received 10 September 2001; accepted for publication 11 September 2001.

*Ph.D. Student, Department of Aerospace Engineering; currently Senior Engineer, T-50 Structural Analysis Team, Korea Aerospace Industries, Ltd., 321, Yuchon Ri, Sanam Myun, Sachon-City, Kyungnam 664-942, Republic of Korea.

†Graduate Research Assistant, Department of Aerospace Engineering.

‡Professor, Department of Aerospace Engineering. Member AIAA.

Introduction

FLUTTER is a dynamic instability phenomenon, and it involves aerodynamic, inertia, and elastic forces of a flight vehicle. If flutter, an aeroelastic problem, occurs in flight, the structures of flight vehicles might fail or the controllability might decrease. Therefore, it is important to predict the aeroelastic characteristics accurately to prevent aeroelastic instabilities of flight vehicles.

Wraparound fins, also called curved fins, which are curved in the spanwise direction, have been used primarily for their advantages in packaging tube-launched projectiles during past decades. These surfaces can be folded against the cylindrical projectile body and be made fit into the launch tube, allowing more efficient use of space. Thus, a greater number of wraparound fin projectiles can be stored in the same space as fixed-fin projectiles designed to deliver the same payload. These wraparound fins, because of their special geometric shapes, produce roll moment even at zero angle of attack, which makes them roll, and the roll direction changes as Mach number varies.[1]

To minimize the effect of aerodynamic and inertial asymmetries on the free-flight trajectory, conventional projectiles as well as wraparound fin projectiles have appropriate roll rates. The flutter characteristics of the projectiles with roll rate are very different from those without roll rate. Because of the roll rate, the roll moments of projectiles are produced, and the dynamic characteristics of fins are varied. Even if a projectile with wraparound fins does not have an initial roll rate, it will start to roll because of the roll moment of the projectile. Because of the roll rate, the wraparound fins are subjected to bending moments by centrifugal and aerodynamic forces, and the spanwise curvature are deformed. In this paper our concern is focused on the roll-rate effects on the flutter characteristics of wraparound fins in the supersonic range, and a computational study was conducted for a wraparound fin with double-wedge fin cross section.

The roll moment coefficient for a nonaxisymmetric body had been predicted using the Euler or Navier–Stokes computational method.[2–4] The steady and unsteady flowfields of rolling projectiles can be observed from a body-fixed coordinate frame.[5] Recently, Paek and Lee[6] calculated roll-producing moment, roll-damping moment, and the equilibrium spin rate of a wraparound fin projectile using Euler equations in body-fixed rotating coordinate frame

including the aeroelastic effects on the roll characteristics. Rivera[7] made an experiment on the flutter of a clamped wraparound fin in subsonic range, but rolling motion was not considered. The present research is considered to be the first flutter analysis for a rolling wraparound fin projectile.

In this paper, the aerodynamic force is computed by solving the Euler equations. The governing equations are appropriately modified to include the coriolis and centrifugal accelerations resulting from the rotating coordinate frame. A finite element modeling of the fin structure and the dynamic analysis of wraparound fin considering the centrifugal force has been performed using the multipurpose finite element code, EMRC/NISA.[8] A static deflection of the wraparound fin is produced by the centrifugal and aerodynamic forces and has been considered previously for a wraparound fin.[6] In the present flutter analysis the static deflection by centrifugal force is small and is ignored for the brief and concise computation and modal analysis is adopted for saving computational time.

For a consistent analysis, a nondimensionalized aeroelastic equation was formulated considering the roll motion. Nondimensionalized aeroelastic parameters, such as velocity index and mass ratio, were devised. For various velocity indices and mass ratios the effects of roll rate on the flutter characteristics of a rolling wraparound fin are studied.

Aerodynamic Model

The Euler equations of a strong conservative form in a generalized coordinate system are given as[6,9]

$$\frac{\partial \hat{Q}}{\partial \tau} + \frac{\partial \hat{F}}{\partial \xi} + \frac{\partial \hat{G}}{\partial \eta} + \frac{\partial \hat{H}}{\partial \zeta} = \hat{S} \tag{1}$$

where the conservative variable vector $\hat{Q}$, the flux vectors $\hat{F}$, $\hat{G}$, and $\hat{H}$, and the source vector $\hat{S}$ are

$$\hat{Q} = J^{-1}[\rho \quad \rho u \quad \rho v \quad \rho w \quad \rho e]^T \tag{2}$$

$$\hat{F} = J^{-1} \times [\rho U \quad \rho u U + \xi_x p \quad \rho v U + \xi_y p \quad \rho w U + \xi_z p \quad \rho U h + U_\Omega p]^T$$

$$\hat{G} = J^{-1} \times [\rho V \quad \rho u V + \eta_x p \quad \rho v V + \eta_y p \quad \rho w V + \eta_z p \quad \rho V h + V_\Omega p]^T \tag{3}$$

$$\hat{H} = J^{-1} \times [\rho W \quad \rho u W + \zeta_x p \quad \rho v W + \zeta_y p \quad \rho w W + \zeta_z p \quad \rho W h + W_\Omega p]^T$$

$$\hat{S} = J^{-1}[0 \quad 0 \quad \Omega^* \rho w \quad -\Omega^* \rho v \quad 0]^T \tag{4}$$

The rotation axis is confined to x axis (Fig. 1) from the projectile nose to the tail, Ω^* is the nondimensional aerodynamic roll rate, and

$$U = \xi_x u + \xi_y v + \xi_z w - U_\Omega, \qquad V = \eta_x u + \eta_y v + \eta_z w - V_\Omega$$
$$W = \zeta_x u + \zeta_y v + \zeta_z w - W_\Omega \tag{5}$$

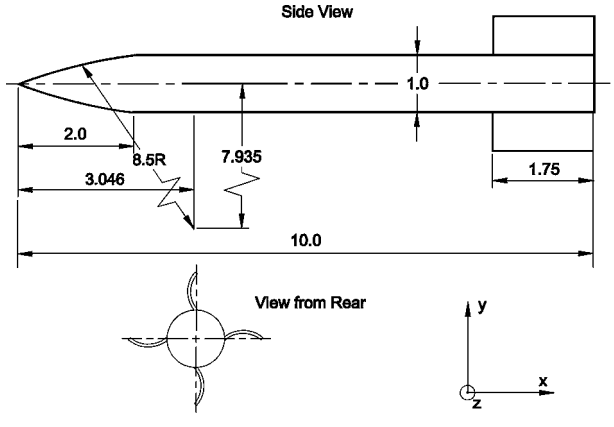

Fig. 1 Geometry of TTCP standard model (in calibers).

$$U_\Omega = \xi_y(-\Omega^* z) + \xi_z(\Omega^* y), \qquad V_\Omega = \eta_y(-\Omega^* z) + \eta_z(\Omega^* y)$$
$$W_\Omega = \zeta_y(-\Omega^* z) + \zeta_z(\Omega^* y) \tag{6}$$

The pressure p and enthalpy h can be related to the dependent variables by applying the ideal gas law

$$p = \rho(\gamma - 1)\left[e - \tfrac{1}{2}(u^2 + v^2 + w^2)\right] \tag{7}$$

$$h = e + p/\rho \tag{8}$$

For a numerical implementation we used the finite volume method for the spatial discretization and the diagonally approximate factorization method by Pulliam and Chaussee[10] for the time integration. A more detailed explanation about the numerical technique is available in Refs. 2 and 9.

Nondimensionalized Aeroelastic Equation

The aeroelastic equation can be written as

$$[M]\{\ddot{u}_s\} + [K]\{u_s\} = \{P(u_s, \dot{u}_s, t)\} \tag{9}$$

where $[M]$, $[K]$, $\{u_s\}$, and $\{P\}$ are the mass matrix, stiffness matrix, structural displacement, and aerodynamic force, respectively. The aerodynamic load vector is changed by the fin deflection and can be written as

$$\{P_a\} = \tfrac{1}{2}\rho_\infty U_\infty^2 \{\Delta C_p A\} \tag{10}$$

where ΔC_p and A are the pressure coefficient difference between convex side and concave side of a curved fin and the area associated with ΔC_p, respectively. From Eqs. (9) and (10) the following nondimensionalized aeroelastic equation can be written as

$$M_0 D\omega_0^2[\bar{M}]\{\ddot{\underline{u}}\} + M_0 D\omega_0^2[\bar{K}(\bar{\Omega})]\{\underline{u}\} = \tfrac{1}{2}\rho_\infty U_\infty^2 D^2\left\{\Delta C_p(\underline{u}, \Omega^*)\bar{A}\right\} \tag{11}$$

The nondimensional roll rate $\bar{\Omega}$ and Ω^* are defined as

$$\bar{\Omega} = \Omega/\omega_0, \qquad \Omega^* = \Omega D/U_\infty \tag{12}$$

A velocity index V_I and a mass ratio μ are defined as follows:

$$V_I = U_\infty \big/ \omega_0 D\sqrt{\mu}, \qquad \mu = 2M_0 \big/ \rho_\infty D^3 \tag{13}$$

Using Eq. (13), Eq. (11) can be rewritten in a more compact form as

$$[\bar{M}]\{\ddot{\underline{u}}\} + [\bar{K}]\{\underline{u}\} = V_I^2\{\Delta C_p \bar{A}\} \tag{14}$$

The nondimensional deflection $\{\underline{u}\}$ can be transformed to the generalized coordinates as follows:

$$\{\underline{u}\} = [\Psi]\{\zeta\} \tag{15}$$

The mass matrix and stiffness matrix are transformed as follows:

$$[\Psi]^T[\bar{M}][\Psi] = [I], \qquad [\Psi]^T[\bar{K}][\Psi] = \left[\bar{\omega}_i^2 \delta_{ij}\right] \tag{16}$$

From Eqs. (15) and (16), Eq. (14) can be written as follows:

$$\ddot{\zeta}_i + \bar{\omega}_i \zeta_i = V_I^2\{\underline{\psi}\}_i^T\{\Delta C_p \bar{A}\} \tag{17}$$

If the jth impulse response $\{\bar{A}\Delta C_p\}_j$ of $\{\Delta C_p \bar{A}\}$ and the amplitude ζ_j of the jth mode are introduced, the generalized aerodynamic force vector $\{\underline{\psi}\}_i^T\{\Delta C_p \bar{A}\}$ can rewritten as follows:

$$\{\underline{\psi}\}_i^T\{\Delta C_p \bar{A}\} = \{\underline{\psi}\}_i^T\left\{\sum_j \bar{A}\Delta C_{pj}^* \zeta_j\right\} = \{\underline{\psi}\}_i^T \sum_j \{\bar{A}\Delta C_p\}_j^* \zeta_j = \sum_j \{\underline{\psi}\}_i^T\{\bar{A}\Delta C_p\}_j^* \zeta_j \tag{18}$$

where * means a convolution integral.

If the motion is harmonic, then Eq. (17) can be transformed by Fourier transform as follows:

$$-\omega^2\zeta_i + \bar{\omega}_i^2\zeta_i = V_I^2 \sum_j C_{ij}\zeta_j \tag{19}$$

where aerodynamic influence coefficient C_{ij} is defined as

$$C_{ij} = \mathcal{F}\left(\{\underline{\psi}\}_i^T\{\bar{A}\Delta C_p\}_j\right) \tag{20}$$

Equation (20) is finally rewritten as follows:

$$-\mu k^2\zeta_i + \frac{\bar{\omega}_i^2}{V_I^2}\zeta_i = \sum_j C_{ij}\zeta_j \tag{21}$$

where the reduced frequency k is a nondimensional frequency related to the aerodynamic force and defined as $k = \bar{\omega}D/U_\infty$.

The V-g (or K-E) and p-k methods[11] are generally used to obtain the flutter solution of Eq. (21). These methods have differences in their formulations but give the same results in flutter computation. Artificial structural damping g is introduced into the flutter equation to use V-g method. The function g is required to stabilize the aeroelastic system in Eq. (21), and the system is unstable if g is positive. Substituting $\bar{\omega}_i$ by $\bar{\omega}_i(1+ig)$, Eq. (21) becomes as follows:

$$-\mu k^2\zeta_i + \bar{\omega}_i^2\lambda\zeta_i = \sum_j C_{ij}\zeta_j \tag{22}$$

where

$$\lambda = (1+ig)\Big/V_I^2 \tag{23}$$

Finally, Eq. (22) can be rewritten as follows:

$$\lambda\{\zeta\} = [A]\{\zeta\} \tag{24}$$

where

$$[A] = \left[\bar{\omega}_i^2\right]^{-1}([C] + \mu k^2[I]) \tag{25}$$

Then, Eq. (24) becomes a complex eigenvalue problem, and matrix $[A]$ is a function of k when Mach number and mass ratio are constant. For various value of k, $\lambda_i (i = 1 \sim n)$ are obtained by solving the eigenvalue problem of Eq. (24). From the definition of eigenvalue λ, the velocity index and structural damping are calculated as follows:

$$V_I = 1\Big/\sqrt{Re(\lambda)}, \qquad g = Im(\lambda)/Re(\lambda) \tag{26}$$

As the velocity index is increased, structural damping g is changed from negative to positive. This point is the flutter point; at this point the velocity index V_I is the flutter velocity index V_{If}, and the frequency $\bar{\omega}(= kU_\infty/D)$ is the flutter frequency $\bar{\omega}_f$.

Divergence is a static instability, and divergence speed can be obtained from Eqs. (24) and (25). When k is 0.0, Eq. (24) can be written as follows:

$$\lambda_D\{\zeta\} = \left[\bar{\omega}_i^2\right]^{-1}[C(k=0)]\{\zeta\} \tag{27}$$

where

$$\lambda_D = 1\Big/V_I^2 \tag{28}$$

$\lambda_{Di} (i = 1 \sim n)$ can be obtained by solving the eigenvalue problem of Eq. (27). From the largest positive value of the real eigenvalues, divergence speed V_{ID} can be calculated as follows:

$$V_{ID} = 1\Big/\sqrt{\lambda_D} \tag{29}$$

Aerodynamics

Three configurations of the model were used in this analysis. The first model was used to compare the roll-producing moment coefficients computed by the present aerodynamic code with the experiment. The second and third models were used for unsteady aerodynamic and flutter analyses. The first model is the same as the standard TTCP (The Technical Cooperation Program) configuration, as shown in Figs. 1 and 2. The basic configuration of the second model is same as the first, but the fin shape, especially the tip shape of the fin, is different, as shown in Fig. 3. The tip shape of the first model is blunt, but the second is sharp. The fin shape of the third model is basically the same as the second, but the body shape is different. The body of the second model is the whole projectile shape, which is a full model, but the third model has its nose removed and the wraparound fins attached at the infinite body, which is a fin-only model. This model is used to save computational time and memory size in the computation of the unsteady aerodynamics. Figure 4 shows the surface mesh of the computational grid system for this model. The grid systems of the projectile model and the

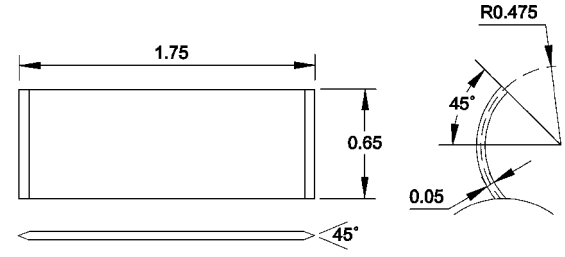

Fig. 2 Fin shape of TTCP standard model (in calibers).

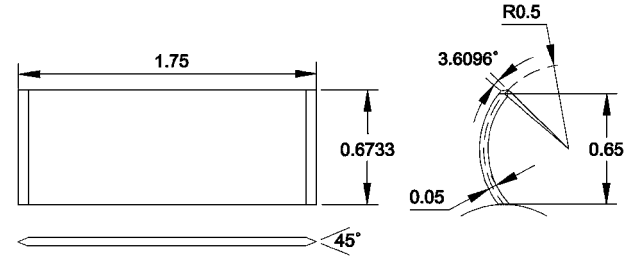

Fig. 3 Fin shape used in the computational model.

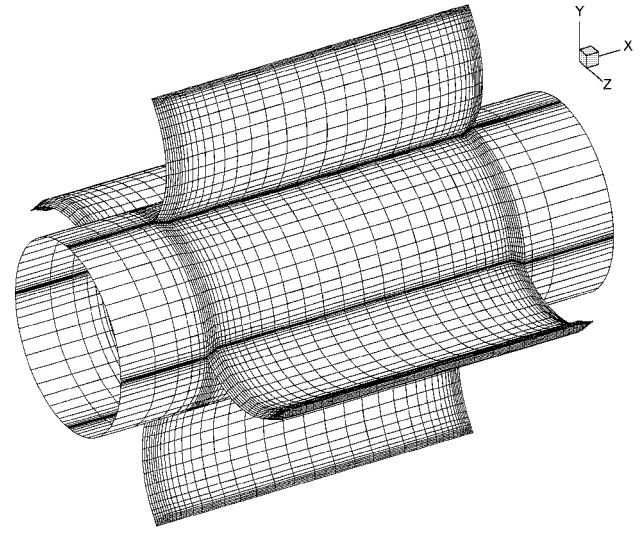

Fig. 4 Surface mesh of the computational grid system for the infinite-body model.

infinite-body model used for the aerodynamic analysis are H-H type, and their dimensions are each ($85 \times 25 \times 41$) and ($51 \times 25 \times 41$), respectively.

The computational domain was taken to be the region including the upper surface (concave side) of one fin and the lower surface (convex side) of the adjacent fin as the boundaries of the domain. Here, this region is referred to as a fin passage. In general, to model the influence of adjacent fins the entire projectile with all of the fins would be needed to be solved. However, for an axisymmetric flowfield considered here all fin passages can be assumed to be identical and symmetric, and only one fin passage needs to be solved with the conditions of symmetry. The experimental data for TTCP standard model used for comparison were obtained from Ref. 12. Figure 5 shows the variation of roll moment coefficient[6] with Mach number. The experimental data were obtained at the Jet Propulsion Laboratory, and computations were made with the present Euler code. Figure 5 shows that the roll moment coefficients computed with the present Euler code agree well with the trend and the magnitude of the experimentally obtained data. Also shown by Edge[12] are the computational results for the same fin configuration except with the blunt leading and trailing edge. Reference 2 can be also referred to as a detailed description and discussion for the roll moment coefficients of this model.

Figure 6 shows the roll moment coefficients of the projectile model and the infinite-body model. The pressure produced on fins of the projectile model is slightly lower than the infinite-body model because of the shock produced at the nose. As shown in Fig. 6, although the roll moment coefficients of the infinite-body model are slightly higher than the projectile model in the positive roll moment region the overall roll moment coefficients of the projectile model and infinite-body model agree well. Therefore, in this paper the infinite-body model is used in the flutter analyses instead of the projectile model to save computational time and memory. The comparison of unsteady aerodynamics between the projectile model and infinite-body model will be presented later.

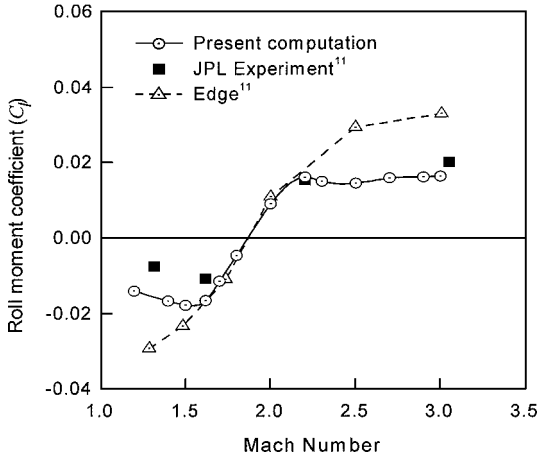

Fig. 5 Roll moment coefficient vs Mach number for computational and Jet Propulsion Laboratory experimental data.

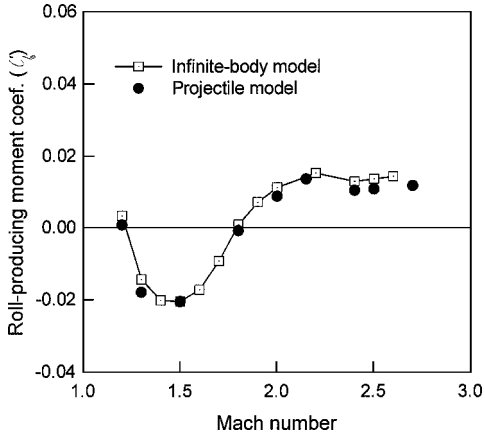

Fig. 6 Comparison of the roll moment coefficients between the projectile model and the infinite-body model.

Vibration Analysis

The basic configuration of a wraparound fin used in this analysis is based on TTCP, as shown in Fig. 3. The fin structure is modeled using 4×8 eight-node quadrilateral general shell elements in the EMRC/NISA code. The material properties of 6061-T6 aluminum alloy and the aerodynamic properties at the sea-level standard condition atmosphere are used to determine appropriate values for nondimensional parameters and are shown in Tables 1 and 2.

Figure 7 shows the variations of the lowest five natural frequencies with roll rate of a wraparound fin. The first mode is the first bending mode (1B), and the second is the first torsion mode (1T). The third mode is the first chordwise bending mode (1C) because the aspect ratio is small. The fourth is the second bending (2B), and the fifth is

Table 1 Structural and aerodynamic properties used for the selection of the aeroelastic parameters

Parameter	Value
Structural properties[a]	
Young's modulus E	70 Gpa
Shear modulus G	29 Gpa
Mass density ρ_s	2860 kg/m^3
Aerodynamic properties[b]	
Speed of sound a	340.3 m/s
Air density	1.225 kg/m^3

[a]Material properties of 6061-T6 aluminum alloy.
[b]Aerodynamic properties at sea level.

Table 2 Parameters computed using the properties of Table 1

Parameter	Value
D	0.1016 m
$M_0 = \rho_s D^3$	3.000 kg
$\omega_0 = \sqrt{(ED/M_0)}$	48,694 rad/s
$\mu = 2M_0/\rho_\infty D^3$	4,669.4
$V_I = U_\infty/\omega_0 D\sqrt{\mu}$	$1.2079^a \times 10^{-3}$
	$\sim 2.6172^b \times 10^{-3}$

[a]Value determined at $M = 1.2$.
[b]Value determined at $M = 2.6$.

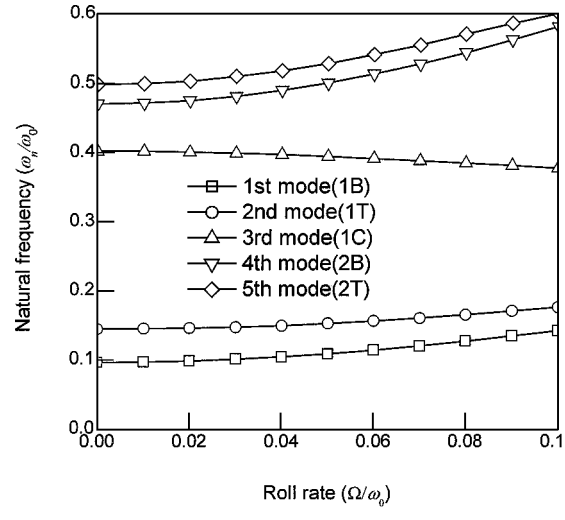

Fig. 7 Variations of natural frequencies with roll rate of a wraparound fin.

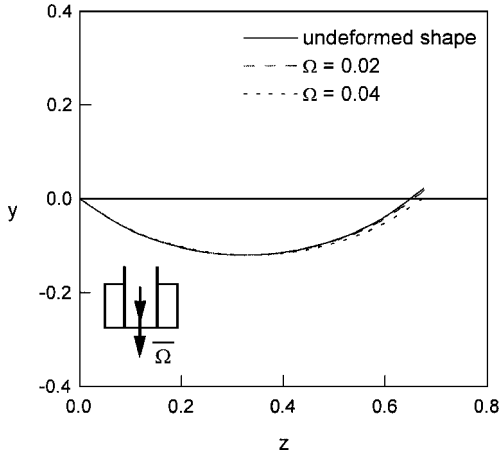

Fig. 8 Variation of static deflection of a wraparound fin with roll rate.

the second torsion (2T). As the roll rate increases, the frequencies of bending and torsion modes increase. This is the stiffening effect by the centrifugal force. However, the frequency of chordwise bending mode (1C) decreases as the roll rate increases. This is because the curvature of wraparound fin decreases and the chordwise bending motion is easy to occur.

Figure 8 shows the static spanwise deflections of a wraparound fin with various roll rates, especially $\bar{\Omega} = 0.00$, $\bar{\Omega} = 0.02$, and $\bar{\Omega} = 0.04$. As shown in Fig. 8, the static deflection of the fin with $\bar{\Omega} = 0.04$, by centrifugal force, is not so small, and it cannot be ignored. However, in this analysis the static deflection is assumed to be small, and the static deflection is ignored in the present flutter analysis when the nondimensional roll rate $\bar{\Omega}$ is smaller than 0.02.

Flutter Analysis

In this flutter analysis for the infinite-body model, modal analysis and V-g method are used to save computational time and memory size. To calculate the aerodynamic influence coefficients, the transient responses are calculated using Euler code when a structure is excited by numerical impulse for a particular mode. Using Fourier transform, the aerodynamic influence coefficients can be obtained from the excited pulse and the transient responses for a particular mode. This method is so called the transient pulse method. Figure 9 shows the flowchart of the transient pulse method, and Fig. 10 shows the road map of the flutter analysis. The number of modes used in the flutter analysis is four.

Figure 11 shows the aerodynamic influence coefficients of the projectile model and the infinite-body model when wraparound fins are in oscillation in the first bending mode. As shown in Fig. 11, the results for the projectile and infinite-body models are in good agreement, but there are some differences in the off-diagonal terms between two models when the reduced frequency k is over 1.0. The magnitudes of the off-diagonal terms in Fig. 11 are small compared with the diagonal term, and the flutter generally occurs in the region where k is under 1.0. Therefore, these differences between two models in Fig. 11 are not so important. Also the influence coefficients for other modes are similar to this case.

Figure 12 shows the results of flutter analysis for the projectile and infinite-body models. In this case the structural models of the two models are same, and only the aerodynamic models are different. As in the preceding predictions, the results of flutter analysis for two models are in good agreement. Therefore, the infinite-body model is used in the following flutter analyses to save computational time and memory.

Flutter analyses of a rolling wraparound fin are performed when Mach number M is 1.6 and 2.5, and $\bar{\Omega}$ is 0.00, 0.01, and 0.02. Roll directions for each Mach number are different from each other because the signs of the roll moment coefficients at $M = 1.6$ and 2.5 are opposite. The sign of the roll moment coefficient at $M = 1.6$ is negative around the x axis, and the sign at $M = 2.5$ is positive.

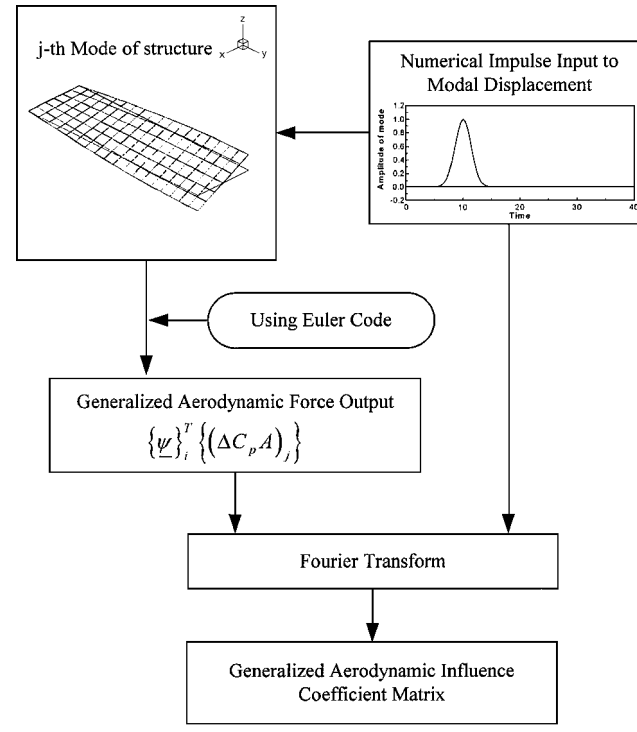

Fig. 9 Flowchart for the computation of generalized aerodynamic influence coefficients.

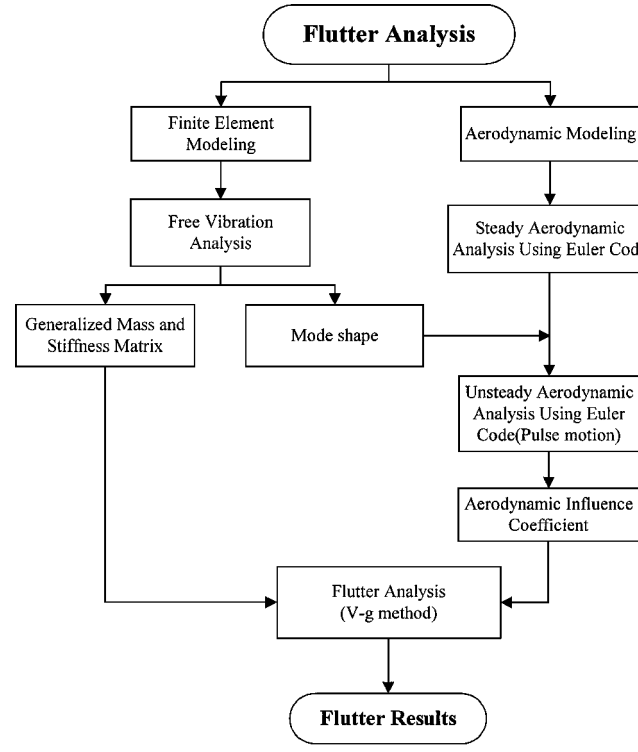

Fig. 10 Road map of flutter analysis using transient pulse method.

Figure 13 shows the results of flutter analysis at $M = 1.6$, where the roll direction is negative. As shown in Fig. 13, the flutter speed increases as the mass ratio increases. This is reasonable because the increase in the mass ratio decreases the dynamic pressure. As the roll rate increases, the flutter speed increases. In general, the flutter speed decreases as the difference of natural frequencies between the first bending mode and the second mode (the first torsion mode) decreases. Although the difference might be small, the frequencies of the first and second mode become more close as the roll rate

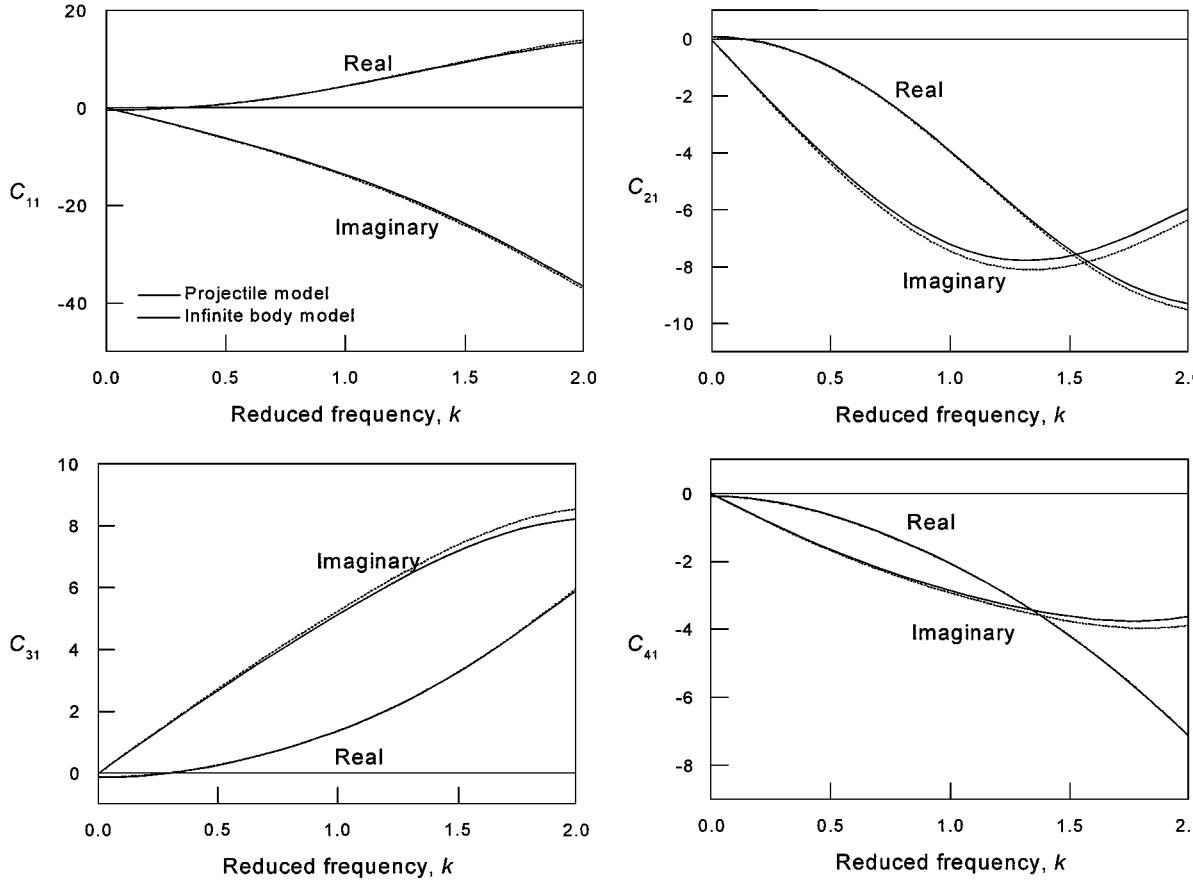

Fig. 11 Aerodynamic influence coefficients for the first natural mode.

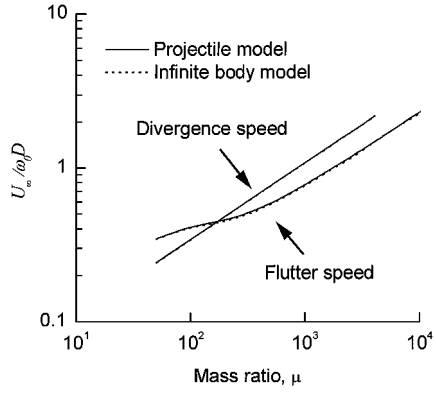

Flutter and divergence speed

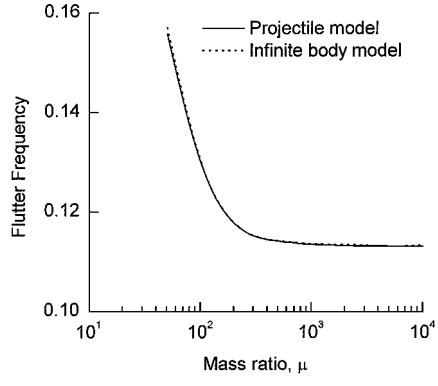

Flutter frequency

Fig. 12 Comparison between the flutter solutions of the projectile model and the infinite-body model ($M = 2.5, \Omega/\omega_0 = 0.0$).

increases. For this structural reason the flutter speed must generally decrease. But the present results are opposite to the general flutter phenomena. These results show that the increase in the flutter speed is made by aerodynamic characteristics of a rolling wraparound fin. The flutter of a wraparound fin is typically mode coalescence flutter. This flutter occurs as the motion of the bending mode accelerates to transfer aerodynamic energy to the torsion mode, and it is important to investigate the bending motion. In steady aerodynamics the shock wave of a concave side is stronger than that of a convex side. This difference causes torsion deformation in the convex direction, and this characteristic of the wraparound fin increases the local angle of attack. The roll in the negative x direction also increases the angle of attack locally. This local increase in angle of attack increases the pressure difference of the leading edge and the trailing edge. These increases of angle of attack make torsion deformation of the curved fin difficult. Therefore, the roll in the negative x direction makes the flutter speed of curved fin increase.

Figure 14 shows the results of flutter analysis at $M = 2.5$ and x directional roll. In this case the divergence speed is also presented because the divergence speed is comparable with the flutter speed. Effects of the mass ratio on flutter characteristics in x directional roll is the same as the preceding case, $-x$ directional roll. Contrary to the preceding case, the flutter speed decreases as the roll rate increases. In contrast to roll in $-x$ direction, the roll rate in x direction decreases the local angle of attack, and this decreases the pressure differences at the leading edge and the trailing edge. Therefore, the roll in x direction decreases the flutter speed of the wraparound fin. The divergence speed increases as the roll rate increases. This is because the divergence happens in the first bending mode, and the centrifugal force increases the bending stiffness. Thus the bending mode becomes more stable. Therefore, the divergence speed of a rolling wraparound fin increases as the roll rate increases.

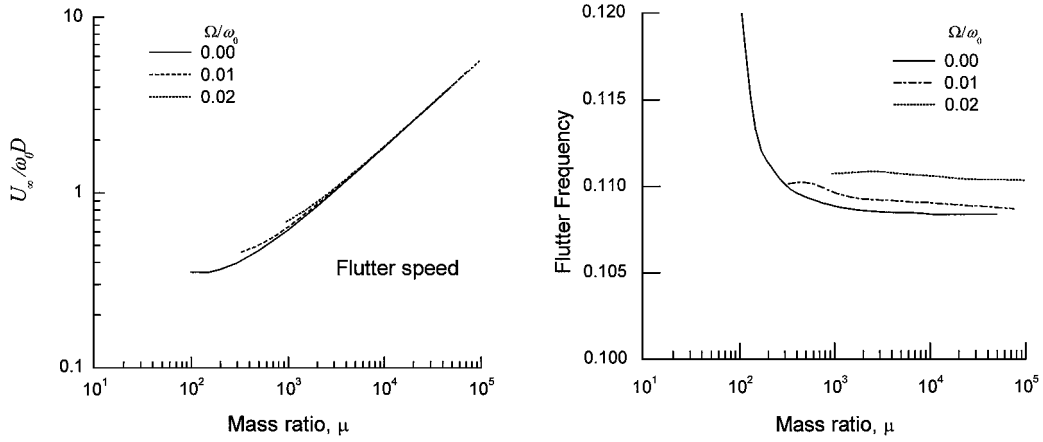

Fig. 13 Variation of flutter solution with mass ratio in negative roll at $M = 1.6$.

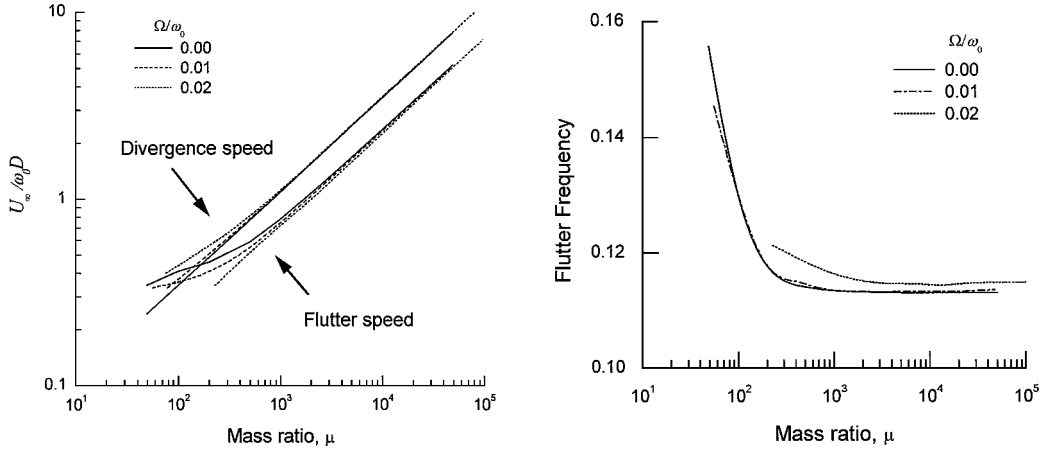

Fig. 14 Variation of flutter solution with mass ratio in positive roll at $M = 2.5$.

Conclusions

The flutter analyses for a projectile with wraparound fins are performed in the supersonic range. This is the first research concerned with the flutter analysis of a rolling wraparound fin. The flowfield is computed by solving Euler equation in a body-fixed rotating coordinate frame. The finite element structure modeling and the free vibration analysis of the curved fin considering roll motion have been made by using the EMRC/NISA code.

For the consistent and efficient analysis the concepts of nondimensionalizing are presented, and a nondimensionalized aeroelastic equation considering the roll motion is derived. Also, aeroelastic parameters, such as velocity and mass ratio, are devised. Using these equations and parameters, flutter analyses of a wraparound fin considering rolling motion are performed. From these results the following conclusions are obtained.

In rolling motion, except for the first chordwise bending mode, natural frequencies of the wraparound fin increase, but natural frequency of the chordwise bending mode decreases. The increase in the roll rate increases the divergence speed of a wraparound fin because the rolling motion of a wraparound fin increases the first bending stiffness.

Flutter characteristics of a curved fin with roll are very different from those without roll and are affected by the roll direction. Roll in negative x direction increases the flutter speed, but roll in x direction decreases the flutter speed because of the geometric asymmetry of a wraparound fin. Flutter analyses in each roll direction indicate that a more stable roll direction exists for flutter.

Acknowledgment

This research was supported by Agency for Defense Development in the Republic of Korea. This support is gratefully acknowledged.

References

[1]Winchenbach, G. L., Buff, R. S., Whyte, R. H., and Hathaway, W. H., "Subsonic and Transonic Aerodynamics of a Wraparound Fin Configuration," *Journal of Guidance and Control*, Vol. 9, No. 6, 1986, pp. 627–632.

[2]Paek, S.-K., Park, T.-S., Bae, J.-S., Lee, I., and Kwon, J.-H., "Computation of Roll Moment for Projectile with Wraparound Fins Using Euler Equations," *Journal of Spacecraft and Rockets*, Vol. 36, No. 1, 1999, pp. 53–58.

[3]Wardlaw, A. B., Priolo, F. J., and Solomon, J. M, "Multiple-Zone Strategy for Supersonic Missiles," *Journal of Spacecraft and Rockets*, Vol. 24, No. 4, 1987, pp. 377–384.

[4]Abate, G. L., and Cook, T., "Analysis of Missile Configurations with Wrap-Around Fins Using Computational Fluid Dynamics," AIAA Paper 93-3631, Aug. 1993.

[5]Schiff, L. B., "Nonlinear Aerodynamics of Bodies in Coning Motion," *AIAA Journal*, Vol. 10, No. 11, 1972, pp. 1517–1522.

[6]Paek, S.-K., and Lee, I., "Aeroelastic Effects on the Roll Characteristics of a Wraparound Fin Projectile," *Journal of Spacecraft and Rockets*, Vol. 36, No. 4, 1999, pp. 524–530.

[7]Rivera, J. A., Jr., "Experimental and Analytical Investigation of the Effect of Spanwise Curvature on Wing Flutter at Mach Number of 0.7," NASA TM 4096, Feb. 1989.

[8]*NISA II USER'S MANUAL*, Engineering Mechanics Research Corp., Troy, MI, Dec. 1996.

[9]Paek, S. K., and Lee, I., "Static Aeroelastic Analysis for Wrap-Around Fins of a Rolling Projectile," *Proceedings of JSASS 11th International Sessions in 35th Aircraft Symposium*, Tokyo, 1997, pp. 647–650.

[10]Pulliam, T. H., and Chaussee, D. S., "A Diagonal Form of an Implicit Approximate Factorization Algorithm," *Journal of Computational Physics*, Vol. 39, No. 2, 1981, pp. 347–363.

[11]Rodden, W. P., and Johnson, E. H., "MSC/NASTRAN Version 68 Aeroelastic User's Guide," MacNeal–Schwendler Corp., March 1994.

[12]Edge, H. L., "Computation of the Roll Moment for a Projectile with Wrap-Around Fins," *Journal of Spacecraft and Rockets*, Vol. 31, No. 4, 1994, pp. 615–620.

P. Weinacht
Associate Editor